Articles

Structure Determination of the Ras-Binding Domain of the Ral-Specific Guanine Nucleotide Exchange Factor Rlf[†,‡]

Dirk Esser,[§] Bettina Bauer,[§] Rob M. F. Wolthuis,[∥] Alfred Wittinghofer,[§] Robbert H. Cool,*[,§] and Peter Bayer[⊥]

Max-Planck-Institut für molekulare Physiologie, Abteilung Strukturelle Biologie, Abteilung Physikalische Biochemie, Rheinlanddamm 201, 44139 Dortmund, Germany, and Laboratory for Physiological Chemistry, Utrecht University, Universiteitsweg 100, 3584 CG Utrecht, The Netherlands

Received May 18, 1998; Revised Manuscript Received July 9, 1998

ABSTRACT: Ral-specific guanine nucleotide exchange factors RalGDS, Rgl, and Rlf have been suggested to function as intermediates between Ras and Ral pathways by being able to bind Ras proteins through their C-terminal Ras-binding domains (RBD). The RBDs of RalGDS and of the Ser/Thr kinase c-Raf-1 have been shown to have the same tertiary structure. In contrast to the RBDs of Raf and RalGDS, which bind either Ras or Rap with high affinity, Rlf-RBD has a similar affinity for both GTP-binding proteins. To be able to compare these RBDs on a structural level, we have solved the three-dimensional structure of Rlf-RBD by NMR spectroscopy. The overall tertiary structure of Rlf-RBD shows the $\beta\beta\alpha\beta\beta\alpha\beta$-fold of the ubiquitin superfamily and is very similar to that of RalGDS-RBD. The binding interface of Rlf-RBD to Ras was mapped using chemical shift analysis and indicated a binding mode similar to that in the case of Rap·Raf-RBD. However, comparison of the putatively interacting regions revealed structural differences which are proposed to be responsible for the different substrate affinities of Rlf-, RalGDS-, and Raf-RBD.

Small GTP-binding proteins such as the Ras protein are essential components of signal transduction pathways responsible for many different biological functions in the cell. They bind guanine nucleotides and their conformation is dependent on the nature of the bound nucleotide, enabling them to function as molecular switches (*1*). In general, only the GTP-bound form can activate the downstream effector in the signal transduction pathway, whereas the GDP-bound form is inactive. The switching between the two conformations is regulated by proteins that stimulate either the slow intrinsic GTP hydrolysis or the slow intrinsic GDP-dissociation rate: GTPase activating proteins (GAPs)[1] or guanine nucleotide exchange factors (GEFs), respectively (*2*).

It has become clear in this decade that many of the signal transduction pathways are not as linear as they initially were thought to be and that Ras proteins can interact with many effector molecules to activate parallel pathways (for references see ref *3*). Besides the Ser/Thr kinase c-Raf-1, one of the earlier examples of Ras effector molecules is the Ral-specific GEF RalGDS. Ral is a small GTPase belonging to the Ras protein family, being 51% identical to Ras (*4*). Although discovered already more than a decade ago, the biological function of Ral has remained elusive for a long period. However, Ral-interacting proteins were isolated in the last years, shedding more light on the function of Ral. In addition to RalGDS (*5*), other Ral-specific GEFs (which we propose to generally name RalGEFs) were identified, that is, Rgl (*6*) and Rlf (*7*). Recently, also the human homologue of Rlf, named RGL2, was identified (*8*, *9*). The isolation of the rabbit oncogene *rsc*, resulting from a fusion between the rabbit homologue of yeast gene *Rad23* encoding a transcription factor with a ubiquitin-like domain, and the gene *rgr*, comprising a RalGDS-like domain with RalGEF activity, shows that components of the Ral pathway can have oncogenic effects (*10*). Ral-specific GTPase activating proteins, named RalGAPs, were partially purified (*11*, *12*), but so far the corresponding genes have not been isolated. A putative effector molecule Rlip (also named RalBP-1 or RIP) was identified, interacting specifically with the GTP-bound form of Ral (*13*−*15*). Rlip also comprises a RhoGAP

[†] Financial support: B.B. and R.H.C. were supported by the EC Grant BIO4-CT96-1110, P.B. by BMFT/DLR.

* Corresponding author. Tel: x-49-231-1206 524. Fax x-49-231-1206 230. E-mail: robbert.cool@mpi-dortmund.mpg.de.

[‡] Atomic coordinates for the Ras-binding domain of mRlf were deposited at the Brookhaven Protein Data Bank under filename 1RLF.

[§] Abteilung Strukturelle Biologie.

[∥] Utrecht University.

[⊥] Abteilung Physikalishe Biochemie.

[1] Abbreviations: Clean-TOCSY, total correlated spectroscopy with suppression of ROESY-type cross-peaks; DQF−COSY, double-quantum-filtered correlated spectroscopy; DSS, 2,2-dimethyl-2-silapentane-5-sulfonate, sodium salt; DTE, dithio-erythritol; ESI-MS, electrospray ionization mass spectrometry; GAP, GTPase activating protein; GEF, guanine nucleotide exchange factor; GSH, reduced glutathione; GST, glutathione-*S*-transferase; HMQC, hetero-multiple-quantum correlation; HSQC, hetero-single-quantum correlation; IPTG, isopropyl-thio-galactoside; NOESY, nuclear overhauser enhancement spectroscopy; RBD, Ras-binding domain; SDS−PAGE, sodium dodecyl sulfate−polyacrylamide electrophoresis; TPPI, time proportional phase incrementation; Tris, tris(hydroxymethyl)aminomethane.

S0006-2960(98)01166-0 CCC: $15.00
Published on Web 09/05/1998

domain with activity toward Rac and Cdc42, suggesting it to be a cross-talking intermediate. In addition, it became clear that Ral is involved in the activation of phospholipase D1 (*16*−*18*).

Double hybrid studies showed that RalGDS is able to interact through its C-terminal moiety with H-, K-, and R-Ras, and Rap1A, an interaction that is affected by specific mutations in the effector domain of these Ras-like proteins (*19*, *20*). Thus, RalGDS binds to the effector region of Ras and Rap similar to the Ras effector and Ser/Thr kinase c-Raf-1, although with different affinities (*21*, *22*). The structure of the Ras-binding domain of c-Raf-1 (Raf-RBD) in complex with Rap1A·GppNHp was solved by crystallography and was shown to have a ubiquitin fold (*23*). Despite a low similarity in primary sequence, the Ras-binding domain of RalGDS (RalGDS-RBD) has an identical topology and a 3D structure highly similar to the Raf-RBD as shown by NMR spectroscopy (*24*) and crystallography (*25*). Mutations in the effector region of Rap indicate that residue 31 is a major contributor to the specificity of the interaction between Ras/Rap and Raf-RBD (*26*).

Recently, the RalGEF Rlf was shown to mediate a Ras-dependent pathway parallel to the Raf/Mek/Erk kinase pathway (*27*) similar to RalGDS (*28*−*30*) and Rgl (*31*). Furthermore, Ral activation was shown to be Ras-dependent in fibroblasts (*32*) and possibly Rap1A-dependent in platelets (*33*). Remarkably, different from Raf-RBD and RalGDS-RBD which bind preferentially Ras or Rap1A, respectively, Rlf-RBD binds to Ras and Rap with similar affinity (*7*). To get a clearer view on the structural basis of the specificity of the interaction between the different RBDs with Ras and Rap, we have solved the structure of Rlf-RBD by NMR spectroscopy. We could identify chemical shifts of specific residues when comparing the spectrum of Rlf-RBD with that of the complex H-Ras$^{1-171}$·GppNHp·Rlf-RBD, suggesting their involvement in the interaction between the two proteins. The structure of Rlf-RBD was compared with that of Raf- and RalGDS-RBD in order to gain insight in structural differences that might be responsible for the biochemical differences of the three RBDs.

MATERIALS AND METHODS

Cloning Procedures and Protein Purification. The original construct of Rlf-RBD (*7*) produced the GST-fused Rlf-RBD (residues Gly646−Arg736) followed by a C-terminal extension of 17 amino acids originating from the pGEX-4T3 vector sequence. To eliminate this extension, the DNA fragment encoding Rlf$^{Gly646-Arg735}$ was recloned in *Bam*HI/*Eco*RI-cleaved pGEX-4T3 (Pharmacia Biotech Inc.) by standard PCR methods using the upstream primer 5′-GGGCCA GGATCCTCTGATTGCCGA-3′ (*Bam*HI restriction site underlined) and the downstream primer 5′-GTGGGAATTC-GGGGTGGCAGCTTAGGGTCATCTGCG-3′ (*Eco*RI restriction site underlined and stop codons indicated by the double underline). It should be noted that the Gly646 and Ser647 were used as part of the thrombin recognition site and that consequently after thrombin cleavage the peptide contains no Rlf alien amino acids. Throughout this paper, the numbering 1−90 was used for residues Gly646−Arg735.

Rlf-RBD was expressed in the protease-poor *Escherichia coli* strain AD202 (ompT::Tn5; ref *34*) on Standard I medium (Merck) at 37 °C. At an OD_{600} of 0.5, expression was induced with 0.5 mM IPTG. After an additional incubation for 5 h at 37 °C, bacteria were harvested by centrifugation and the pellet was stored at −20 °C. For sample preparation, a cell pellet was resuspended in a 3-fold excess (volume buffer/weight cells) of buffer A (PBS, pH 7.4, 5 mM DTE, 14 mM β-mercaptoethanol, 0.1 mM Pefablock (Sigma)) and the cells were lysed by sonication. Unsoluble and high molecular weight particles were separated by centrifugation (1 h at 40000*g*). The supernatant was used for the purification procedure as described previously (*7*). The suspension was loaded on a GSH−Sepharose column (Pharmacia Biotech Inc.) pre-equilibrated with buffer A, and then the nonbinding proteins were eluted by washing with the same buffer. Rlf-RBD was cleaved from the GST fusion part by incubation with thrombin (10 NIH units/expected mg of fusion protein) in buffer B (50 mM Tris-HCl, pH 7.6, 50 mM NaCl, 5 mM DTE) overnight at 4 °C. After elution with buffer B and SDS−PAGE analysis of the fractions, the pooled fractions were concentrated to approximately 5 mg/mL and loaded on a gel filtration chromatography column (Superdex75, 26/60; Pharmacia), pre-equilibrated with 50 mM Tris-HCl, pH 7.6, 100 mM NaCl, 5 mM DTE. The fractions containing highly purified Rlf-RBD were concentrated to 2 mM, dialyzed against 50 mM Tris-HCl, pH 7.6, and 5 mM DTE, snap-frozen in aliquots in liquid nitrogen, and stored at −80 °C. The protein yield was 16 mg/L of medium. ^{15}N-labeled protein was purified according to the same procedure mentioned above but by using Vogel-Bauer minimal medium and bacterial strain BL21(DE3) for the protein production. Isotopically enriched agents were obtained from Aldrich (Germany), all others from Merck or Sigma (Germany).

For the PCR cloning of the RBD of the mouse protein Rgl (amino acids 635−735) into pGEX-4T3, we used as template the yeast shuttle vector pPC86-Rgl, which was isolated in a two-hybrid screen using the mouse PC86-cDNA library and human Rap1A as bait (*7*). The oligonucleotides in the PCR reaction were the following: upstream primer 5′-CCATTGGATCCACAGTACTGCCTCCTG (*Bam*HI restriction site underlined; please note that the codon for Ser635 lies within the *Bam*HI restriction site) and the downstream primer 5′-CCGAATTCGCAACTTCACCTG-CTACTACTACGAG (*Eco*RI restriction site underlined and stopcodons indicated by the double underline). Sequencing showed that the codon for residue 662 (AAC, encoding Asn) differed from the published codon (CAC, encoding His; ref *6*). Similarly, the homologous position in RalGDS is Asn. The overproduction and purification procedure of the Rgl-RBD was performed as described above for Rlf-RBD.

K-Ras, N-Ras, and H-Ras$^{1-171}$ were kindly donated by Dorothee Vogt. The (m)GppNHp-bound form of the Ras proteins was prepared by incubation of the purified Ras-(-like) protein with alkaline phosphatase and a 2-fold excess of (m)GppNHp, followed by separation of nonbound nucleotide from the Ras protein by gel filtration as described before (*35*). The mGppNHp-bound forms of mutants Ras-(T35A), Ras(E37G), and Ras(Y40C) were a kind gift of Petra Grünewald.

Determination of Substrate Affinity. The interaction between the RBDs of Rlf and Rgl and the mGppNHp-bound forms of Ras and Rap1A were determined by fluorescence

Table 1: Comparison of the Dissociation Constants of the Interaction of Several RBDs and Their Substrates

substrate	Rlf-RBD (μM)	Rgl-RBD (μM)	RalGDS-RBD[a] (μM)	Raf-RBD[a] (μM)
H−Ras	0.09	3.5	1.0	0.02
K−Ras	0.06	3.6	nd[b]	0.04
N−Ras	0.21	1.5	nd[b]	0.04
Rap1A	0.27	nd[b]	0.01	1.2
H−Ras(T35A)	≫5	nd[b]	nd[b]	nd[b]
H−Ras(E37G)	0.26	nd[b]	nd[b]	3.4
H−Ras(Y40C)	≫5	nd[b]	nd[b]	nd[b]

[a] Refs *24* and *26*. [b] nd: not determined.

spectroscopy as described before (*7*, *21*) in 50 mM Tris-HCl, pH 7.6, 5 mM $MgCl_2$, 5 mM DTE, and 5% glycerol at 37 °C using the Perkin-Elmer fluorometer LS50B (excitation wavelength 366 nm, emission wavelength 450 nm). Active site titration using 1.5 μM of Ras·mGppNHp showed that 64% of the Rlf-RBD was active. The calculated dissociation constants as given in Table 1 were corrected for this percentage.

Sample Preparation for NMR Spectrometry. Fifty microliters of ^2H_2O (99.9%) was added to 450 μL of a 2 mM solution of Rlf-RBD (50 mM sodium phosphate, pH 6.5, 0−100 mM NaCl) and filled in a 5 mm sample tube for NMR analysis. Spectra of the Rlf-RBD·Ras^{1-171}·GppNHp complex (components Rlf-RBD and Ras^{1-171}·GppNHp mixed with molar ratio 1:1.2, respectively) were recorded with a sample containing a 1 mM protein solution.

Sample Quality. The monomeric state of the protein and homogeneity of the sample were routinely tested before and after recording of NMR spectra by gel filtration, SDS−PAGE analysis, and electrospray mass spectroscopy (Finnigan). ESI-MS measurements were also applied to determine the isotopical enrichment of the protein.

NMR Measurements. NMR measurements were performed on a Bruker DRX-500 spectrometer equipped with shielded z gradients. The temperature was set to 300 K. All experiments are listed in Table 2. For picking hydrogen bonds within the protein, 2D NOESY spectra were recorded 6 h after dissolving a lyophylized sample in ^2H_2O. DSS was used as an internal standard for calibration of the proton resonances. For ^{15}N calibration we followed the procedure of Wishart et al. (*36*).

Processing, analysis, and visual representation of the 2D and 3D spectra were done using the NDEE program package (*37*) on Indy workstations (Silicon Graphics Inc.). Spectra were recorded in the phase-sensitive absorption mode with the TPPI method. The time domain data for ^1H and ^{15}N frequencies were zero-filled once or twice prior to Fourier transformation. 2D spectra were acquired with 2048−8096 data points in the f2 dimension and 512−1024 data points in the f1 dimension. The water resonance was suppressed by applying the WATERGATE sequence (*38*) or by presaturation. HSQC spectra were processed using a Blackman filter (NDEE program package) with a frequency cutoff at the water resonance and a down-sampling rate of 2. Prior to Fourier transformation all spectra were multiplied with a sine bell square window function shifted by p/3 or p/4.

Structure Calculation. A family of 50 structures was calculated by a simulated annealing (SA) approach followed by a refinement procedure using the X-PLOR program package 3.1 (*39*). For calculation only slightly changed standard protocols have been used (soft potential during SA and square-well potential during refinement). Distances from NOEs, coupling constants, and hydrogen bridges were introduced to the simulated annealing approach in a step-by-step procedure. Initially only sequential and medium-range NOEs as well as long-range NOEs defining the β-sheet areas and coupling constants have been used for structure calculation. All other long-range NOEs and hydrogen bridges were introduced in consecutive steps. Finally the intraresidual NOEs were accepted. Back-calculation was applied during several rounds of the refinement procedure. All structures were calculated on the basis of a repel function. Additional refinements using electrostatic interactions ($\epsilon = 3$) did not change the overall structure (salt bridges, hydrogen bonds, secondary structure, etc.) and were therefore neglected.

Table 2: List of NMR Experiments[a]

experiment	M (ms)	purpose	literature
^1H-^1H-DQF−COSY		coupling constants, assignment of spin systems	*61*
^1H-^1H−NOESY	100	distance information	*62*
^1H-^1H−NOESY	200	distance information, assignment of spin systems	*62*
NOESY (^2H_2O)	200	distance information, hydrogen bonds	*62*
Clean-TOCSY	100	assignment of spin systems	*63*
^{15}N−HSQC		assignment of NH, coupling constants	*64*
^{15}N−NOESY−HMQC	100	assignment of spin systems, distance information	*65*
^{15}N-TOCSY−HMQC	100	assignment of spin systems	*66*

[a] The mixing times (M), purposes, and literatures of all experiments performed with unlabeled or labeled (98% ^{15}N) samples of Rlf-RBD are given. All measurements were done at a pH of 6.5 and at a temperature of 300 K.

Distances and Dihedral Angle Restraints. All NOEs were extracted from the 2D NOESY spectra as well as from the 3D NOESY−HMQC. An r^{-6} dependence was assumed for calibrating distances from NOE data. NOE intensities were calculated by the amplitude of the cross-peak maximum (*40*) and subdivided in three different classes: strong (1.8−2.7 Å), medium (1.8−4.0 Å), and weak (1.8−5.5 Å). The intensity of the Hd/He NOE of Tyr21 was used as a calibration standard (2.5 Å). Pseudo-atom corrections (*41*) were performed prior to structure calculation using a simple FORTRAN program. To avoid overestimation of NOE intensities due to a contribution of zero-quantum coherence, all intraresidual NOEs between vicinal protons were allowed to cover a distance range of 1.8−4.0 Å. Coupling constants were fitted from double-quantum-filtered COSY and ^{15}N-^1H-HSQC spectra using a crude or simplex algorithm (NDEE program package). The standard error due to resolution and fitting was about 1.0−1.5 Hz. ϕ dihedral angles were calibrated from $^3J_{NH-Ha}$ coupling constants using the Karplus relationship (*42*). The constraints were set to $-120 \pm 40°$ (>7.5 Hz) and $-60° \pm 20°$ (<6 Hz).

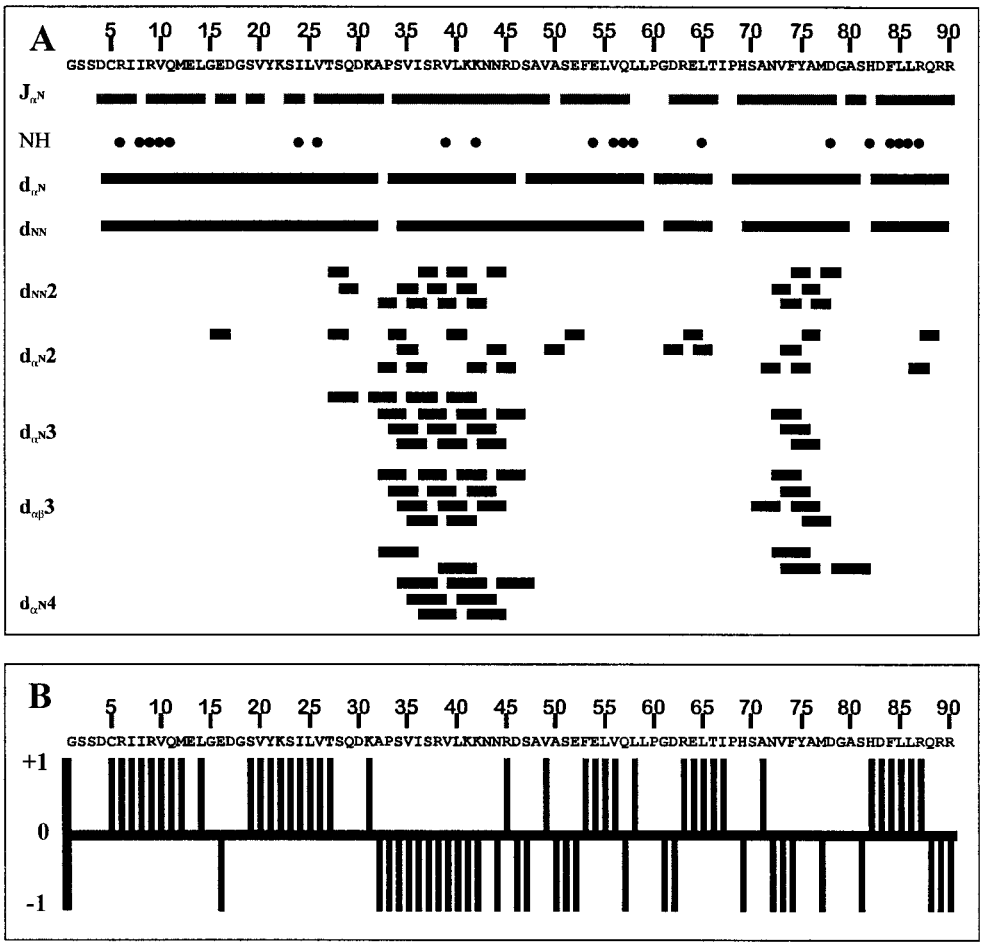

FIGURE 1: Secondary structure determination. (A) NOE pattern: Sequential and medium-range NOEs typical for secondary structure as well as $^3J_{\alpha N}$ coupling constants are indicated as black bars. Filled circles indicate NH protons not exchanged after 6 h in ^2H_2O. (B) Chemical shift index plot: Chemical shifts of Hα protons differing more than ±1 from their random coil shifts are denoted as black bars. A local "density" of 4 or more "−1" bars not interrupted by a "1" indicates an α-helix; any "dense" grouping of three or more "+1" bars not interrupted by a "−1" is a β-sheet.

Hydrogen Bonds and Salt Bridges. Hydrogen bonds were defined by standard parameters (*43*) setting two NOEs for each backbone hydrogen bond. After structure calculation we ran X-PLOR programs to search for atom distances and angles favorable for hydrogen bonds and salt bridges (*44*). The selection parameters for hydrogen bonds were distances below 2.6 Å and N−NH·O═C angles smaller than 60°. Forsalt bridges we chose a distance of smaller than 4 Å between O^- and N^+.

Definition of Secondary Structure. *Wishart Plot*. For calculation of the chemical shift index we followed the procedure of Wishart et al. (*45*), using their revised data (*46*). Corrections due to amino acids followed by a proline were done.

Constraints. For the characterization of the secondary structure due to distance and angle constraints we preferentially used NH-H$\alpha_{i,i+3}$, NH-H$\alpha_{i,i+4}$, and Hα_i-Hβ_{i+3} (α-helices) and long-range NOEs of consecutive amino acids in stretched regions (β-sheet). Additionally ϕ dihedral angles and nonexchangeable NH protons were included to analyze the structural elements. *DSSP*. The program DSSP (*47*) was used to find α-helices, β-sheets, and turn and coil conformations.

RESULTS

Biochemical Analysis of the Substrate Specificity. We have reported before (*7*) that the dissociation constants of Rlf-RBD for H-Ras and Rap1A were similar, respectively 0.6 and 0.4 μM. Since the construct were used for that study comprised a C-terminal extension of the RBD by 17 amino acids originating from the pGEX vector sequence, we determined the dissociation constants of the newly isolated Rlf-RBD described in this work. The dissociation constants for Ras and Rap are still very similar, 0.09 and 0.27 μM, respectively (Table 1), but differ from the values reported for the older construct, especially the dissociation constant for Ras binding. There could be two reasons for these differences: the presence of the C-terminal extension in the earlier construct of Rlf-RBD protein and/or differences in the assay buffer; in this work we added 5% glycerol to the buffer in order to stabilize the proteins. However, the presence of 5% glycerol is not responsible for the increased affinity for Ras, since the dissociation constant of the former, C-terminally extended Rlf-RBD construct for H-Ras·mGppNHp was determined to be 0.8 μM in glycerol-containing buffer (cp. to 0.6 μM in buffer without glycerol). Consequently, the C-terminal extension apparently affects the substrate affinity, most likely in an indirect way.

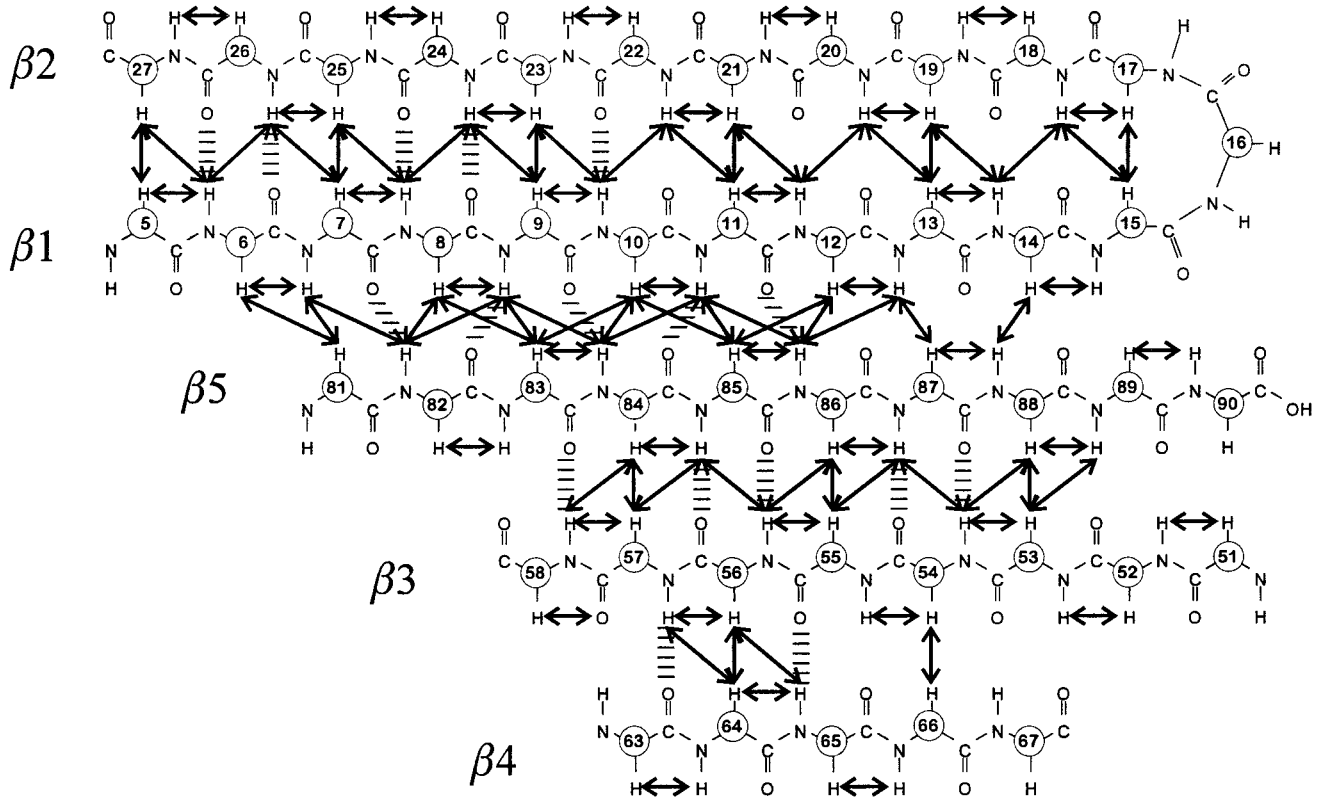

FIGURE 2: Secondary structural elements: β-sheet pattern in Rlf-RBD showing five b-strands being antiparallel with the exception of $\beta1-\beta5$. NOEs between backbone protons are indicated by black arrows.

The affinities of Rlf-RBD for the three Ras isoforms (K_D = 0.06−0.21 μM) and for Rap1A (K_D = 0.27 μM) are in the same order of magnitude. In contrast, Rgl-RBD shows a preferential binding to Rap1A, similar to RalGDS-RBD and inversed to the preference of Raf-RBD (Table 1).

We also tested the effects of some mutations in the effector region of Ras on the interaction with Rlf-RBD. Mutation E37G, which was shown to practically abrogate binding of Ras to Raf, whereas not to RalGDS (*29*, *48*, *49*), affected the interaction between Rlf-RBD and Ras only 3-fold (Table 1). Thus, in this aspect the interaction of Rlf with Ras is more similar to that of RalGDS than to that of Raf. Mutants H-Ras(T35A) and H-Ras(Y40C) did not show any binding up to 5 μM Rlf-RBD (Table 1). In comparison, in two-hybrid analysis these mutations were shown to abrogate the interaction with Raf, adenylate cyclase, and byr2 (*48*, *50*), and mutation Y40C was shown to affect the interaction with RalGDS and Rgl (*48*).

NMR Spectrometry: Resonance Assignments. The sequence-specific resonance assignment of the 90 amino acid Rlf-RBD was achieved according to the standard method developed by Wüthrich (*51*). Spin systems were obtained from 2D DQF−COSY and 2D Clean-TOCSY spectra. 3D ^{15}N-TOCSY−HMQC spectra were recorded to avoid ambiguous assignment of overlapping resonances, although this was not a general problem as the resolution in the fingerprint region was very high. Sequential connectivities were obtained from 2D NOESY spectra with a mixing time of 200 ms and from a 3D ^{15}N-NOESY−HMQC with a mixing time of 100 ms. We chose the strong Arg90 NH−Hα signal as a reliable starting point for the assignment of the C-terminus. Thereafter, Ala32 and Pro33 could be assigned and were taken to trace helix α1 (Ala32−Asn43) which could preferably be assigned by the ^{15}N-^{1}H spectra. The low field shifted fingerprint resonances of amino acids V10, T27, L55, E64, and F84 were used as starting points for the β-sheet characterization. Proline assignments were favorably done by using the connectivities of their Hδ resonances and the Hα peaks of the previous amino acid. The assignment could be solved unequivocally; no unassigned resonances have been left. Cross-peaks for Gly1 to Ser3 could not be found within the recorded TOCSY and COSY spectra. Additionally the NH cross-peak of Ile67 was not visible but could be traced via the NOESY spectrum.

Secondary Structure of Rlf-RBD. Figure 1A shows the NOE pattern of short- and medium-range NOEs defining the secondary structure. The regions of Ala32 to Asn43 and Asn72 to Met77 show typical NOEs (NH_i-NH_{i+2}; $H\alpha_i$-NH_{i+2}; $H\alpha_i$-NH_{i+3}; $H\alpha_i$-NH_{i+4}) arising in an α-helical conformation. Three in D_2O slowly exchanging NH protons (Val39, Lys42, Asp78) could also be found within these regions pointing out that protection—probably due to hydrogen bonding in α-helices—occurs. The existence of helices α-1 and α-2 was confirmed by calculation of the coupling constants. $^{3}J_{NH-Ha}$ couplings defining the ϕ angles of the protein are significantly smaller than 6 Hz in these regions, as expected for an α-helical structure.

Coupling constants higher than 7.5 Hz and long-range NOEs were used to define the β-strands running from amino acids Cys5-Glu13 (β1), Ser19-Thr27 (β2), Phe53-Gln57 (β3), Arg63-Leu65 (β4), and His82-Gln88 (β5). These secondary structural elements were additionally traced by 20 slowly exchanging NH protons listed in Figure 1A. The RBD therefore consists of a five-stranded mixed β-sheet, where all strands are antiparallel with the exception of strands β1 and β5 (Figure 2). The strand character of β4 is poorly

Table 3: Structural Statistics and Coordinate Precision of Ten Favorable Structures

structural statistics and coordinate precision	⟨SA⟩
average total energy (kcal/mol)	503 ± 34
average VdW energy[a] (kcal/mol)	72 ± 12
rms deviation from idealized covalent geometry[b]	
angles (deg)	0.83 ± 0.002
bonds (Å)	0.005 ± 0.0003
impropers (deg)	0.73 ± 0.03
rms deviation of experimental distance restraints (Å)	0.024 ± 0.002
rms deviation of experimantal dihedral restraints (deg)	0.22 ± 0.05
coordinate rms deviation (Å)	
⟨SA⟩ to $\overline{\langle SA \rangle}$ backbone atoms (4−90)[c]	0.20 ± 0.034
⟨SA⟩ to $\overline{\langle SA \rangle}$ all nonhydrogen atoms (4−90)	0.6 ± 0.1

[a] VdW energies were calculated on the basis of a repel function with hard VdW spheres of atoms using the CHARMM force field. [b] Distance violations of the structures were smaller than 0.72 Å (maximum of 5 >0.5 Å) and dihedral angle violations lower than 6°. ⟨SA⟩ is an ensemble of 10 structures obtained by a simulated annealing (SA) procedure and a consecutive refinement. [c] $\overline{\langle SA \rangle}$ is the mean structure calculated of the individual SA structures using a least-squares Fit Program of X-PLOR. N, Cα, and C′ of the backbone or all nonhydrogen atoms of residues 4 to 90 were used for the calculation.

defined by only a few NOEs and coupling constants.

Confirmation of the detected secondary structure comes from the chemical shift index (CSI) method developed by Wishart et al. (*45*). A CSI plot for the resonances of Rlf-RBD is shown in Figure 1B. Consecutive areas of indices of +1 indicate a β-sheet structure, and indices of −1 indicate an α-helix. The regions found in this approach generally overlap very well with those found by NOEs and $^3J_{NH-Ha}$ couplings. However, the CSI method and $H\alpha_i$-$N\beta_{i+3}$ NOEs suggested that the N-terminus of helix α1 started with Ala32. Moreover, the C-terminus of β4 is located at Ile67 when applying the CSI method.

As a second method, we used the program DSSP (*47*) for an independent search for secondary structural elements. α-Helices running from Val35−Asn43 and Phe74−Met77 as well as b-strands from Cys5−Met12, Lys23−Thr27, Phe53−Val56 and His82−Gln88 were found. Strand β4 was not detected by this program.

Taking into account these results, we defined the secondary elements as follows: β1 (Cys5−Met12), β2 (Tyr21−Thr27), α1 (Ala32−Asn43), β3 (Phe53−Gln57), β4 (Arg63−Thr66), α2 (Asn72−Asp78), and β5 (His82−Gln88).

Quality of the 3D Structure. The 3D structure was calculated as described in Material and Methods. For the simulated annealing approach we used 2287 NOE constraints including 718 long-range, 296 medium-range, 469 sequential, and 804 intraresidual NOEs. Thus, as an average every amino acid is characterized by 16.5 contacts to its neighbors. Seventy-four coupling constants and 20 hydrogen bonds were introduced during the structure calculation. With a few exceptions of some glycine residues, the ϕ and ψ values of Rlf-RBD were within the allowed regions of the Ramachandran plot (not shown). In all structures no distance deviations of greater than 0.32 Å and dihedral angle deviations higher than 6.2° from idealized geometry occurred. Approximately 80% of all NOEs could be used for distance calculations. Only some NOEs arising from side-chain resonances in the aliphatic region have been excluded due to spectral overlap. Table 3 shows a statistical overview of the structural characteristics of 10 favorable models of Rlf-RBD. The very low ⟨rmsd⟩ value (0.20 and 0.60 Å) calculated over thebackbone (N, Cα, C′) and over all C, N, O, and S atoms from amino acids 4 to 90 proves the tertiary fold of the protein to be very well defined.

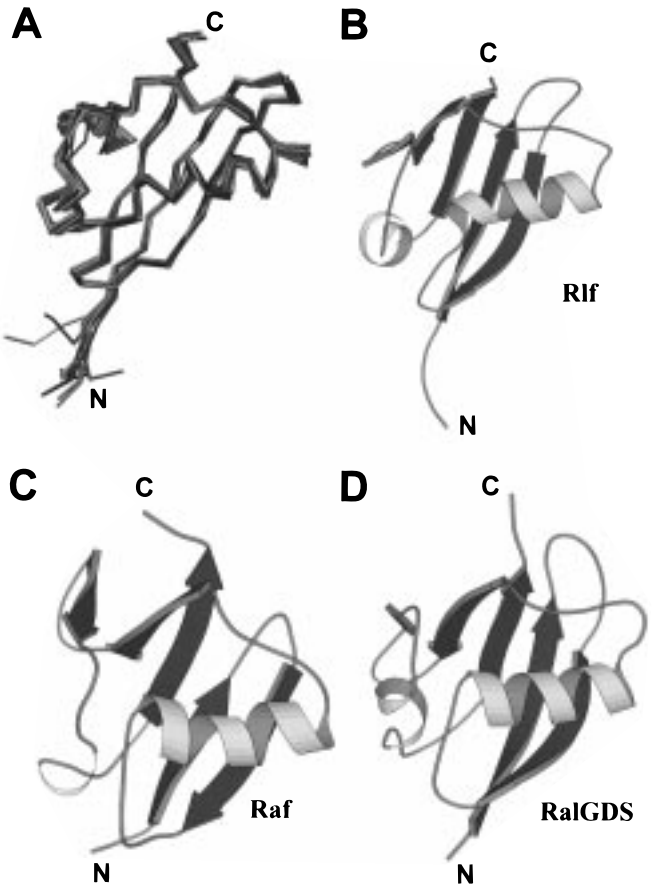

FIGURE 3: The NMR structure of Rlf-RBD compared to those of the Raf- and RalGDS-RBD. (A) Superimposition of 10 backbone structures of Rlf-RBD: Ten backbone structures were superimposed using the group fit algorithm of the sybyl program package (Sybyl, Vers. 6.1, Tripos Inc., Bethesda, MO) for visualization. (B) Molscript representation of the Rlf-RBD structure. (C) Molscript representation of the Raf-RBD structure (*57*). (D) Molscript representation of the RalGDS-RBD structure (*24*).

Description of the Tertiary Fold. The dipole moment of the amphiphatic helix α1 (Ala32−Asn44) is rotated approximately 45° relative to the first β-sheet (β1−β2). Relevant contacts in this region occur between the hydrophobic side chains of Ile8, Val10, Met12, Lys22, and Ile24 (β-strand) and Ala32, Val35, Ile36, Val39, and Leu40 (α-helix). Long-range NOEs were observed from the N-terminal Lys31 of helix α1 to the N-terminus of helix α2 (Asn72, Val73), pushing both helices into a conformation perpendicular to each other. Helix α2 consists of approximately 7 amino acids. The five-stranded β-sheet of Rlf-RBD forms a structure resembling a cupped hand, similar to Raf-RBD. Only strand β4 is twisted against the plane of this sheet. Numerous backbone interactions in addition to salt bridges (Arg6−Ser28; Arg6−Asp78; Arg9−Ser23) stabilize the tertiary fold of Rlf-RBD. A superposition of 10 backbone structures is given in Figure 3A. Only amino acids Gly1, Ser2, Ser3, and Asp4 are fading out. This could

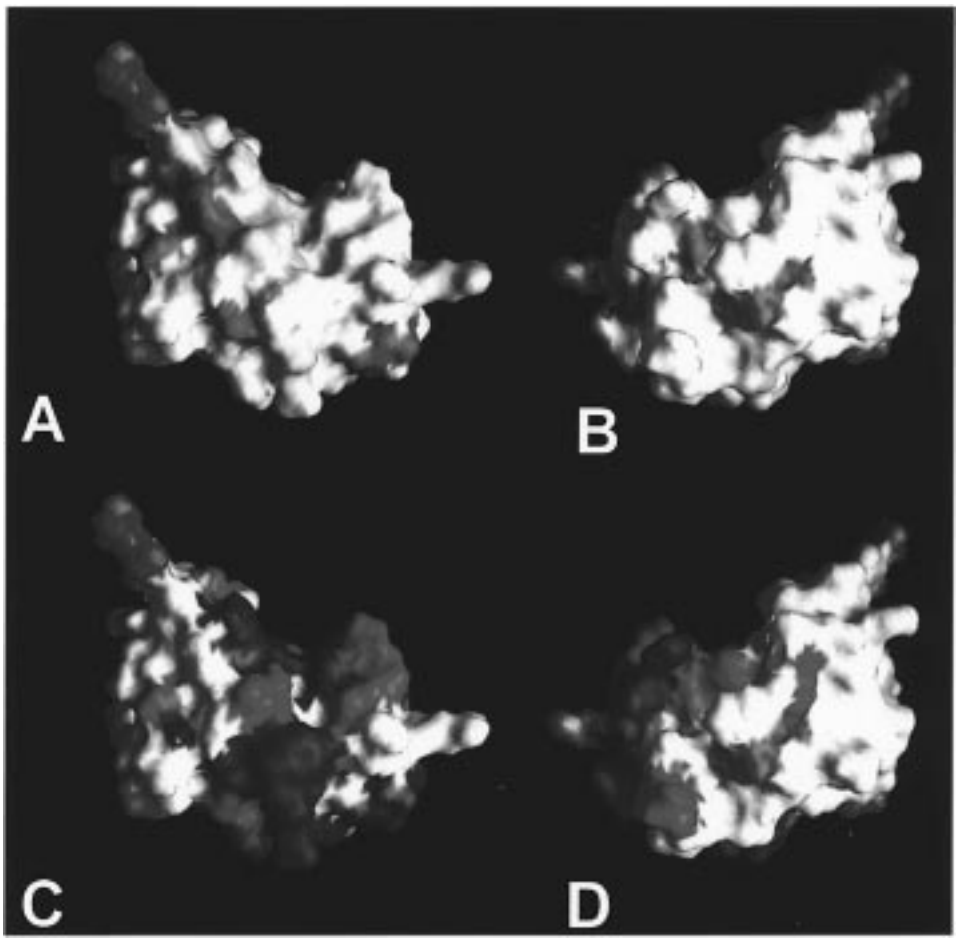

FIGURE 4: Proton and ^{15}N shifts in Rlf-RBD upon binding of Ras^{1-171}·GppNHp. Proton shifts (A, B: 0.03−0.05 ppm, pink; 0.06−0.08 ppm, red; 0.09−1.0 ppm, magenta) and ^{15}N shifts (C, D: 0.15−0.5 ppm, cyan; 0.6−1.0 ppm, blue; 1.1−1.5 ppm, violet) are marked with colors in a Grasp representation of Rlf-RBD. Residues that cannot show shift are marked in green (see text), and residues that did not shift are marked in white (proton shift <0.02 ppm; ^{15}N shift < 0.14 ppm). Rlf-RBD is presented in the same orientation as in Figure 4B (A, C) or turned over 180° (B, D).

probably be due to lacking assignments or structural flexibility. A molscript representation of the backbone structure is given in Figure 3B.

Complex of Rlf-RBD with Ras^{1-171}·GppNHp. To obtain information on the binding of Ras to Rlf-RBD, HSQC spectra of free ^{15}N-labeled Rlf-RBD and bound to Ras^{1-171}·GppNHp were superimposed in the multiplot modus of NDEE to analyze chemical shift differences of the resonances due to complex formation. As expected, all resonance shifts were broadened in the complex. Figure 4 shows a quantitative interpretation of the results. Small shifts were observed for 16 residues, but were considered to be too small to be significant. Stronger shifts ($\geq$0.1 ppm in ^{15}N and/or $\geq$0.05 ppm in ^{1}H) were observed for 44 resonances, representing 53% of the total (shifts can theoretically be measured for 83 residues: 90 minus the 3 N-terminal residues and Ile67, which could not be observed in the TOCSY spectra, and minus the 3 prolines which lack the NH). The shifting resonances are clustered in the stretches Lys31 to Ala50 of helix α1 and the ensuing loop 3; Asp4 to Gln29 of β-strands β1 and β2, and their connecting loop 1; and Asp83 to Arg87 in strand β5.

DISCUSSION

In this work, we present the NMR structure of the Ras-binding domain of the Ral-specific exchange factor Rlf. Rlf-RBD, like the RBDs from c-Raf-1, RalGDS, and Rgl, is able to bind to Ras and Rap proteins. The RBDs of the three RalGEFs were suggested to be important in Ral-mediated signal transduction pathways, which were demonstrated to be Ras-dependent and parallel to the Raf/MEK/Erk pathway (*16*, *27*, *30*, *31*, *52*, *53*). Rlf seems to differ from the other RalGEFs and from Raf-RBD in its affinity for Ras and Rap proteins: whereas RalGDS-RBD and Rgl-RBD have a high affinity for Rap1A and an approximately 100-fold lower affinity for H-Ras (Table 1; refs *22*, *54*), and Raf-RBD shows a high affinity for Ras and a 100-fold lower affinity for Rap1A (*21*), Rlf-RBD has a similar, intermediate affinity for both proteins (Table 1). Remarkably, mutation E37G in Ras, which abrogates the interaction with c-Raf-1 but not with RalGDS (*29*), hardly affects the interaction of Rlf-RBD, indicating the Ras-binding mode of Rlf-RBD to be more similar to that of RalGDS-RBD than of Raf-RBD. These aspects make the elucidation of the structure of the Rlf-RBD and the comparison with the structures of Raf-RBD and RalGDS-RBD highly interesting.

Similar to Raf- and RalGDS-RBD, the structure of Rlf-RBD shows a ubiquitin superfold, characterized by a $\beta\beta\alpha\beta\beta$-type tertiary structure. This common motif is found in many proteins of different origin with various cellular functions, for example, the algae Fe_2-S_2 ferredoxin and the streptococcal protein G (*44*, *55*, *56*). The RBDs of RalGDS, Rgl,

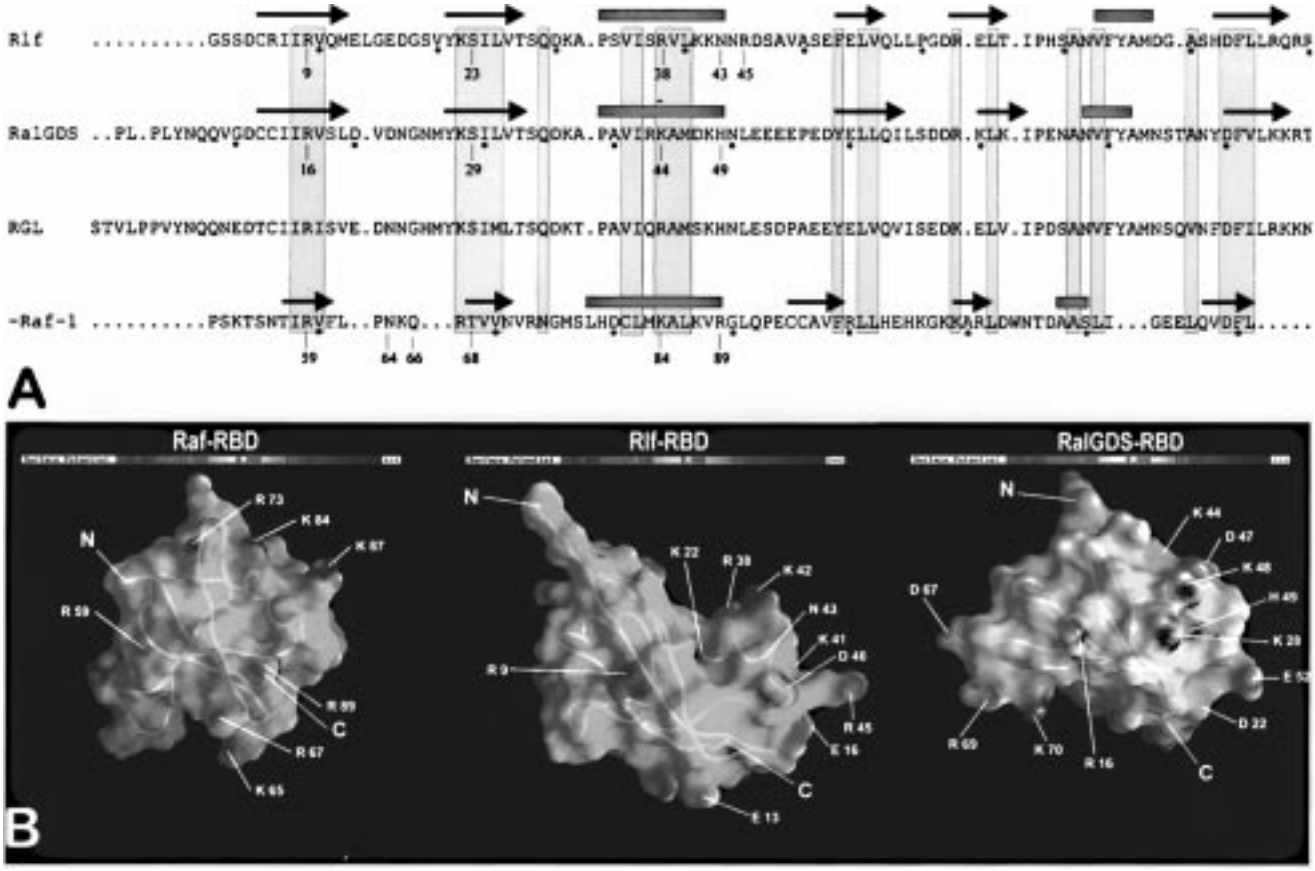

FIGURE 5: Multiple sequence alignment and surface eletrostatic potential. (A) Comparison of sequences of different Rlf-RBD homologuous proteins using the program PileUp (Wisconsin Package Version 8.1, Genetic Computer Group (GCG), Madison, WI) using the parameters: GapWeight = 1.0 and GapLengthWeight = 0.1. The structural elements as found in the NMR structures of the 3 RBDs (see also Figure 3) are indicated with arrows (β-strands) and bars (α-helices). Some residues are indicated with their number (see text). (B) Electrostatic representation of the surface potentials of the RBDs of c-Raf-1, Rlf, and RalGDS (left to right) as calculated with the program Grasp (*67*). Charged residues in proximity to the substrate-binding region are numbered (see text).

and Rlf are characterized by a high sequence homology, but in comparison, Raf-RBD exhibits only a very low degree of similarity. However, when taking the secondary elements into account, the similarity between these RBDs becomes evident (Figure 5A). In Figure 3, we show a molscript representation of the NMR structures of Raf- (*57*), RalGDS- (*24*), and Rlf-RBD in a similar orientation, clearly demonstrating their similarity.

The 3D structure of the complex between Raf-RBD and Rap1A was determined by X-ray crystallography (*23*, *26*) and demonstrated the involvement of a number of amino acids in this interaction. The interacting regions in Raf-RBD lie in the first two β-strands and their connecting loop 1, and in the C-terminal moiety of helix α1. Direct side chain interactions are provided by Raf-RBD residues R59, N64, Q66, T68, and R89 (*23*), whereas K84 was found to interact with E31 and D33 in the complex of Raf-RBD with the Rap1A(E30D,K31E) mutant (*26*). Sequence alignment indicates that to a certain extent similar residues are found in Rlf and RalGDS (Figure 5A), suggesting that the mode of binding of RalGDS- and Rlf-RBD to Ras/Rap resembles the mode found in the Raf-RBD·Rap complex. This hypothesis is strengthened by the observation of resonance shifts in HSQC spectra of Rlf-RBD resulting from the binding to Ras·GppNHp (Figure 4). Shifts were indeed observed in helix α1 and the ensuing loop 3, and in the first two β-strands and the connecting loop 1. Additionally, shifts were observed in strand β4. However, since the β-strands form a large sheet (Figure 2), it would not be surprising when shifts in β1 and β2 would cause indirect effects in other parts of the sheet. A similar pattern of chemical shifts was observed upon binding of Ras to RalGDS-RBD (*24*).

Even though the different RBDs thus seem to bind their substrates by the same mode of interaction, deviations in the structural arrangements and/or in the primary structures have to be responsible for the differences in substrate affinities. A striking difference between the RalGDS-, Rgl-, and Rlf-RBD on one hand (RalGEF-RBDs), and the Raf-RBD on the other hand is the longer loop 1 connecting the strands β1 and β2 observed for the RalGEF-RBDs: Rlf has the longest and Raf the shortest interconnecting loop. Since the primary sequences of these loop regions differ for all RBDs (Figure 5A), and since in Raf-RBD this loop comprises N64 and Q66 that provide polar groups for hydrogen bonds with Rap (*23*), local differences may be critical for the substrate affinity.

Residue E37 in Ras appears to interact with R59 and R67 of Raf (*49*, *58*). Sequence alignment indicates residues R16 in RalGDS-RBD and R9 in Rlf-RBD to be homologous to R59 in Raf (Figure 5A), which is also underlined by the similar positions of these residues in the three RBD structures (Figure 5B). In contrast, although the alignment indicates that residues K28 in RalGDS-RBD and K22 in Rlf-RBD are homologous to R67 in Raf, the three-dimensional position

of these residues relative to the plane of the β-sheet composed by strands β1 and β2 is opposite to that of R67 (Figure 5B). This deviation may explain the fact that mutation E37G in Ras strongly affects the interaction with Raf, but not with RalGDS or Rlf.

Another important region implied in substrate binding is the C-terminal moiety of helix α1. Sequence alignment indicates that K84 in Raf is homologous to K44 in RalGDS-RBD and R38 in Rlf-RBD (Figure 5A). K84 in Raf was shown to be important for the interaction with residues E31 and D33 of Rap1A(D30E/K31E) (*26*). Whereas residue D33 is conserved in Ras and Rap, these proteins differ in position 31, being a glutamate in Ras and a lysine in Rap1A. It was shown that the position 31 is a key residue for the substrate specificity of the Raf- and RalGDS-RBD (*26*, *59*). It is therefore surprising that the sequence and structural similarities of these RBDs indicate that the homologue of Raf K84 in RalGDS-RBD is also a lysine: K44 (Figure 5A). Furthermore, mutation D30E/E31K does not seem to affect the binding of Ras to Rlf-RBD (*60*), indicating that E31 is less important for binding of Ras to Rlf as compared to Raf. These aspects will have to be dealt with by solving the three-dimensional structures of the complexes of the RalGEF-RBDs with the substrates Ras and Rap.

Another helical residue of Raf-RBD that plays an important role in the binding to Rap1A is R89 which forms a salt bridge with the conserved residue D38 (*23*, *26*, *58*). Raf R89 aligns to H49 in RalGDS-RBD and N43 in Rlf-RBD (Figure 5A), neither of which can be involved in salt bridge formation. However, in the three RalGEF-RBDs, the preceding lysine may function similarly after structural rearrangements upon substrate binding.

The electrostatic surface representation of the NMR structures of the 3 RBDs (Figure 5B) shows that the RalGEF-RBDs have a strongly negatively charged region, comprising residues from the loops 1 and 3, whereas this region is hardly charged in Raf-RBD. The chemical shifts that result from the binding of Ras to Rlf-RBD indicate that this region is indeed involved in binding (Figure 4). Remarkably, Rlf-RBD has a positively charged residue in this region: R45. Neither RalGDS- nor Rgl-RBD has a basic residue in this region. It is therefore tempting to speculate that R45 may play a role in binding Ras and might be (partially) responsible for the differences in substrate affinities found between Rlf and the other two RalGEFs.

ACKNOWLEDGMENT

We gratefully thank Bernhard Griewel for help with the NMR spectrometer, Michael Hess for help with Figures 3−5, Petra Grünewald and Dorthee Vogt for proteins, Heino Prinz for mass spectrometric analysis, Christian Herrmann, Sabine Wohlgemuth, and Susanne Metzger for fruitful discussion, and Roger S. Goody for continuous support.

SUPPORTING INFORMATION AVAILABLE

Additional data are available comprising a list of hydrogen bonds and of $^3J_{HN-H\alpha}$ coupling constants, and a figure of the HSQC spectrum plus assignments and of the chain tracing of amino acids H82 to R90 in the fingerprint region (5 pages). Ordering information is given on any current masthead page.

REFERENCES

1. Bourne, H. R., Sanders, D. A., and McCormick, F. (1990) *Nature 348*, 125−132.
2. Boguski, M. S., and McCormick, F. (1993) *Nature 366*, 643−654.
3. McCormick, F., and Wittinghofer, A. (1996) *Curr. Opin. Biotechnol. 7*, 449−456.
4. Chardin, P., and Tavitian, A. (1986) *EMBO J. 5*, 2203−2208.
5. Albright, C. F., Giddings, B. W., Liu, J., Vito, M., and Weinberg, R. A. (1993) *EMBO J. 12*, 339−347.
6. Kikuchi, A., Demo, S. D., Ye, Z.-H., Chen, Y.-W., and Williams, L. T. (1994) *Mol. Cell. Biol. 14*, 7483−7491.
7. Wolthuis, R. M. F., Bauer, B., Van't Veer, L. J., De Vries, M. M., Cool, R. H., Spaargaren, M., Wittinghofer, A., Burgering, B., and Bos, J. L. (1996) *Oncogene 13*, 353−362.
8. Peterson, S. N., Trabalzini, L., Brtva, T. R., Fischer, T., Altschuler, D. L., Martelli, P., Lapetina, E. G., Der, C. J., and White, G. C., II (1996) *J. Biol. Chem. 271*, 29903−29908.
9. Herberg, J. A., Beck, S., and Trowsdale, J. (1998) *J. Mol. Biol. 277*, 839−857.
10. D'Adamo, D. R., Novick, S., Kahn, J. M., Leonardi, P., and Pellicer, A. (1997) *Oncogene 14*, 1295−1305.
11. Emkey, R., Freedman, S., and Feig, L. A. (1991) *J. Biol. Chem. 266*, 9703−9706.
12. Bhullar, R. P., and Seneviratne, H. D. (1996) *Biochim. Biophys. Acta 1311*, 181−188.
13. Jullien-Floris, V., Dorseuil, O., Romero, F., Letourneur, F., Saragosti, S., Berger, R., Tavitian, A., Gacon, G., and Camonis, J. H. (1995), *J. Biol. Chem. 270*, 22473−22477.
14. Cantor, S. B., Urano, T., and Feig, L. A. (1995) *Mol. Cell. Biol. 15*, 4578−4584.
15. Park, S.-H., and Weinberg (1995) *Oncogene 11*, 2349−2355.
16. Jiang, H., Luo, J.-Q., Urano, T., Frankel, P., Lu, Z., Foster, D. A., and Feig, L. A. (1995) *Nature 378*, 409−412.
17. Luo, J.-Q., Liu, X., Hammond, S. M., Colley, W. C., Feig, L. A., Frohman, M. A., Morris, A. J., and Foster, D. A. (1997) *Biochem. Biophys. Res. Commun. 235*, 854−859.
18. Schmidt, M., Voss, M., Thiel, M., Bauer, B., Grannass, A., Tapp, E., Cool, R. H., De Gunzburg, J., Von Eichel-Streiber, C., and Jakobs, K. H. (1998) *J. Biol. Chem. 273*, 7413−7422.
19. Spaargaren M., and Bischoff, J. R. (1994) *Proc. Natl. Acad. Sci. U.S.A. 91*, 12609−12613.
20. Hofer, F., Fields, S., Schneider, C., and Martin, G. S. (1994) *Proc. Natl. Acad. Sci. U.S.A. 91*, 11089−11093.
21. Herrmann, C., Martin, G. A., and Wittinghofer, A. (1995) *J. Biol. Chem. 270*, 2901−2905.
22. Herrmann, C., Horn, G., Spaargaren, M., and Wittinghofer, A. (1996) *J. Biol. Chem. 271*, 6794−6800.
23. Nassar, N., Horn, G., Herrmann, C., Scherer, A., McCormick, F., and Wittinghofer, A. (1995) *Nature 375*, 554−560.
24. Geyer, M., Herrmann, C., Wittinghofer, A., and Kalbitzer, H. R. (1997) *Nat. Struct. Biol. 4*, 694−699.
25. Huang, L., Weng, X., Hofer, F., Martin, S., and Kim, S.-H. (1997) *Nat. Struct. Biol. 4*, 609−615.
26. Nassar, N., Horn, G., Herrmann, C., Block, C., Janknecht, R., and Wittinghofer, A. (1996) *Nat. Struct. Biol. 3*, 723−729.
27. Wolthuis, R. M. F., de Ruyter, N. D., Cool, R. H., and Bos, J. L. (1997) *EMBO J. 16*, 6748−6761.
28. Urano, T., Emkey, R., and Feig, L. A. (1996) *EMBO J. 15*, 810−816.
29. White, M. A., Vale, T., Camonis, J. H., Schaefer, E., and Wigler, M. H. (1996) *J. Biol. Chem. 271*, 16439−16442.
30. Miller, M. J., Prigent, S., Kupperman, E., Rioux, L., Park, S.-H., Feramisco, J. R., White, M. A., Rutkowski, J. L., and Meinkoth, J. L. (1997) *J. Biol. Chem. 272*, 5600−5605.
31. Murai, H., Ikeda, M., Kishida, O., Okazaki-Kishida, M., Matsuura, Y., and Kikuchi, A. (1997) *J. Biol. Chem. 272*, 10483−10490.
32. Wolthuis, R. M. F., Zwartkruis, F., Moen, T. C., and Bos, J. L. (1998) *Curr. Biol. 8*, 471−474.
33. Wolthuis, R. M. F., Franke, B., Van Triest, M., Bauer, B., Cool, R. H., Camonis, J. H., Akkerman, J.-W., and Bos, J. L. (1998) *Mol. Cell. Biol. 18*, 2486−2491.

34. Nakano, H., Yamazaki, T., Ikeda, M., Masai, H., Miyatake, S., and Saito, T. (1994) *Nucleic Acids Res. 22*, 543−544.
35. Lenzen, C., Cool, R. H., and Wittinghofer, A. (1995) *Methods Enzymol. 255*, 95−109.
36. Wishart, D. S., Bigam, C. G., Yao, J., Abildgaard, F., Dyson, H. J., Oldfield, E., Markley, J. L., and Sykes, B. D. (1995) *J. Biomol. NMR 6*, 135−140.
37. Herrmann, F. (1997) NDEE program package for n dimensional NMR data processing and evaluation, Vers. 2.03, Biosymbiose GmbH, Bayreuth, Germany.
38. Piotto, M., Saudek, V., and Sklenar, J. (1992) *J. Biomol. NMR 2*, 661−665.
39. Brünger, A. T. (1993) X-PLOR version 3.1, Howard Hughes Medical Institut and Yale University, New Haven, CT.
40. Barsukov, I. L., and Lian, L.-Y. (1993) in *NMR of Macromolecules* (Roberts, G. C. K., Ed.) Oxford University Press, Oxford.
41. Wüthrich, K., Billeter, M., and Braun, W. (1983) *J. Mol. Biol. 169*, 949−961.
42. Karplus, M. (1959) *J. Chem. Phys. 30*, 11−15.
43. Kraulis, P. J., Clore, G. M., Nilges, M., Jones, T. A., Petterson, G., Knowles, J., and Gronenborn, A. M. (1989) *Biochemistry 28*, 7241−7257.
44. Baumann, B., Sticht, H., Schärpf, M., Sutter, M., Haehnel, W., and Rösch, P. (1996) *Biochemistry 35*, 12831−12841.
45. Wishart, D. S., Sykes, B. D., and Richards, F. M. (1992) *Biochemistry 31*, 1647−1651.
46. Wishart, D. S., Bigam, C. G., Holm, A., Hodges, R. S., and Sykes, B. D. (1995) *J. Biomol. NMR 5*, 67−81.
47. Kabsch, W., and Sander, C. (1983) *Biopolymers 22*, 2577−2637.
48. Khosravi-Far, R., White, M. A., Westwick, J. K., Solski, P. A., Chrzanowska-Wodnicka, M., Van Aelst, L., Wigler, M. H., and der, C. J. (1996) *Mol. Cell. Biol. 16*, 3923−3933.
49. Jaitner, B., Becker, J., Linnemann, T., Herrmann, C., Wittinghofer, A., and Block, C. (1997) *J. Biol. Chem. 272*, 29927−29933.
50. White, M. A., Nicolette, C., Minden, A., Polverino, A., Van Aelst, L., Karin, M., and Wigler, M. H. (1995) *Cell 80*, 533−541.
51. Wüthrich, K. (1986) in *NMR of Proteins and Nucleic Acids*, Wiley, New York.
52. Koyama, S., Chen, Y.-W., Ikeda, M., Muslin, A. J., Williams, L. T., and Kikuchi, A. (1996) *FEBS Lett. 380*, 113−117.
53. Okazaki, M., Kishida, S., Hinoi, T., Hasegawa, T., Tamada, M., Kataoka, T., and Kikuchi, A. (1997) *Oncogene 14*, 515−521.
54. Ikeda, M., Koyama, S., Okazaki, M., Dohi, K., and Kikuchi, A. (1995) *FEBS Lett. 375*, 37−40.
55. Orengo, C. A., Jones, D. T., and Thornton, J. M. (1994) *Nature 372*, 631−634.
56. Ponting, C. P., and Benjamin, D. R. (1996) *Trends Biolchem. Sci. 21*, 422−425.
57. Emerson, S. D., Madison, V. S., Palermo, R. E., Waugh, D. S., Scheffler, J. E., Tsao, K.-L., Kiefer, S. C., Liu, S. P., and Fry, D. C. (1995) *Biochemistry 34*, 6911−6918.
58. Block, C., Janknecht, R., Herrmann, H., Nassar, N., and Wittinghofer, A. (1996) *Nat. Struct. Biol. 3*, 244−251.
59. Shirouzu, M., Morinaka, K., Kpyama, S., Hu, C.-D., Hori-Tamura, N., Okada, T., Kariya, K.-i., Kataoka, T., Kikuchi, A., and Yokoyama, S. (1998) *J. Biol. Chem. 273*, 7737−7742.
60. O'Gara, M. J., Zhang, X.-F., Baker, L., and Marshall, M. S. (1997) *Biochem. Biophys. Res. Commun. 238*, 425−429.
61. Rance, M., Sørensen, O. W., Bodenhausen, G., Wagner, G., Ernst, R. R., and Wüthrich, K. (1983) *Biochem. Biophys. Res. Commun. 117*, 479−485.
62. Kumar, A., Wagner, G., Ernst, R. R., and Wüthrich, K. (1980) *Biochem. Biophys. Res. Commun. 95*, 1−6.
63. Griesinger, C., Otting, G., Wüthrich, K., and Ernst, R. R. (1988) *J. Am. Chem. Soc. 110*, 7870−7872.
64. Grzesiek, S., and Bax, A. (1993) *J. Am. Chem. Soc. 115*, 12593−12594.
65. Fesik, S., and Zuiderweg, E. (1990) *Q. Rev. Biophys. 23*, 97−131.
66. Clore, G. M., and Gronenborn, A. M. (1991) *Prog. NMR Spectrosc. 23*, 32−92.
67. Nicholss, A., Sharp, K. A., and Honig, B. (1991) *Proteins: Struct., Funct., Genet. 11*, 281−296.

BI9811664